Unsteady Compressed Williamson Fluid Flow Behavior under the Influence of a Fixed Magnetic Field (Numerical Study)

AMINE EL HARFOUF[1, *], RACHID HERBAZI[2,3,4], SANAA HAYANI MOUNIR[1],
HASSANE MES-ADI[5], ABDERRAHIM WAKIF[6]
[1]Multidisciplinary Laboratory of Research and Innovation (LaMRI),
Energy, Materials, Atomic and Information Fusion (EMAFI) Team,
Polydisciplinary Faculty of Khouribga,
Sultan Moulay Slimane University,
MOROCCO

[2]Intelligent Systems and Applications Laboratory (LSIA), EMSI,
Tangier,
MOROCCO

[3]ENSAT, Abdelmalek Essaâdi University,
Tangier,
MOROCCO

[4]ERCMN, FSTT, Abdelmalek Essaâdi University,
Tangier,
MOROCCO

[5]Laboratory of Process Engineering, Computer Science and Mathematics,
National School of Applied Sciences of the Khouribga University of Sultan Moulay Slimane,
MOROCCO

[6]Faculty of Sciences Aïn Chock, Laboratory of Mechanics,
Hassan II University,
Casablanca,
MOROCCO

**Corresponding Author*

Abstract: - A numerical investigation is conducted into a two-dimensional mathematical model of magnetized unsteady incompressible Williamson fluid flow over a sensor surface with fixed thermal conductivity and external squeezing accompanied by viscous dissipation effect. Based on the flow geometry under consideration, the current flow model was created. The momentum equation takes into consideration the magnetic field when describing the impact of Lorentz forces on flow behavior. The energy equation takes varying thermal conductivity into account while calculating heat transmission. The extremely complex nonlinear, unstable governing flow equations for the now under investigation are coupled in nature. Due to the inability of analytical or direct methods, the Runge-Kutta scheme (RK-4) via similarity transformations approach is used to tackle the physical problem under consideration. The physical behavior of various control factors on the flow phenomena is described using graphs and tables. For increasing values of the Weissenberg parameter and the permeable velocity parameter, the temperature boundary layer thickens. As the permeable velocity parameter and squeezed flow index increased, the velocity profile shrank. The velocity profile grows as the magnetic number rises. Squeezed flow magnifying increases the Nusselt number's magnitude. Furthermore, the extremely complex nonlinear complex equations that arise in fluid flow issues are quickly solved by RK-4. The current findings in this article closely align with the findings that have been reported in the literature.

Key-Words: - thermal conductivity, Williamson fluid, sensor surface, magnetic field, Weissenberg number.

Received: February 13, 2023. Revised: November 26, 2023. Accepted: December 26, 2023. Published: February 29, 2024.

1 Introduction

Owing to the significant advancements in contemporary technology, careful consideration has been paid to examining the heat transfer properties of squeezing flows in a variety of shapes. In numerous scientific and engineering domains, including polymer processing, food engineering, injection molding, lubrication systems, foam formation, blood flow inside vessels, cooling towers, bi-axial expansion of bubble boundaries, hydrodynamical machines, compression, moisture migration, chemical engineering, dampers, heating/cooling processes, and many more, squeezed flows have many important practical and industrial applications. Nonetheless, the squeezing flow is caused by the typical stresses that are applied to the moving surfaces or plates.

[1], [2], has a thorough overview of the literature and applications related to squeezing flows. The movement of the human body's diarthrodial joints and valves, which is related to the fields of mathematical bioengineering and biomedicine, is another noteworthy illustration of squeezing flow, [3]. In today's biological and chemical technologies, sensors that use stretching surfaces as sensing elements are crucial for identifying a wide range of illnesses, dangerous substances, and biological warfare elements. The issues are addressed in practice by employing a micro-cantilever that bends when target molecules bind to one of its surfaces with the receptor coating. It is evident that in practice, the micro-cantilever is typically positioned in a film of thin fluidic cells with an external squeezing disturbance; this physical scenario of fluid motion over a micro-cantilever is modeled as flow about a sensor surface. Literature, [4], [5] provides a thorough analysis of micro-cantilever, electrochemicals, biosensors, and their applications in diverse biomedical domains. Heat transfer problems, however, have many scientific applications in the field of engineering sciences, including conduction of heat in tissues, thermal energy storage, laser cooling, magnet, and radiative cooling, cooling of nuclear reactors, metallurgical processes, space cooling, and petroleum industries. By creating a mathematical model, [6], significantly advanced the field of squeezing flows in this approach. Later, a lot of researchers carried on with Stefan's problem by considering various geometries with appropriate adjustments. The authors [7], assumed that the length between the plates changed as the inverse square root of time to study the thermodynamic behavior of squeezed flow between two elliptic parallel plates. Additionally, the two-point boundary value problem was modeled in the literature, [8] and is currently being solved utilizing appropriate mathematical techniques such as the homotopy analysis method (HAM) and perturbation scheme. Their research demonstrates that a boundary layer with very little viscosity forms on the plates at higher squeezed number values. The magnetized squeezing flow of a viscous incompressible electrically conducting fluid film created between two parallel discs was investigated, [9]. Additionally, their research assumes that the lower disc will rotate at a temporary, arbitrary angular velocity. Additionally, the typical Hermitian finite difference scheme is used in the literature, [10], to produce numerical solutions. Their analysis did reveal, however, that the torque on the bottom disc is amplified by increasing angular velocity and magnetic number as well as by lengthening the distance between the plates, which increases the load. In this work, [11], investigated the problem of incompressible rectilinear time-dependent, two-dimensional magnetized viscous squeezed flow via an infinite channel using a homotopy analysis approach. They find that the viscous behavior of the fluid under consideration can be explained by a diminishing magnetic field. The analytical solution of the squeezing flow between circular plates was addressed in [12], using semi-numerical techniques as the homotopy analysis method. Furthermore, the crossflow behavior on the axial velocity profile is shown by the improved Reynolds number. In this work, [13], the authors used HAM to study the issue of incompressible transient viscous squeezed flow of two-dimensional fluid between two parallel plates under the influence of chemical reaction and viscous dissipation. According to the literature, [13], the magnifying squeezing number raises the momentum transmission coefficient and decreases the concentration field. The magnetized time-dependent, two-dimensional, incompressible, pair stress microfluid flow between two parallel plates with chemical reaction effects was established in [14]. According to their research, the heat field decreases as the squeezing flow parameter increases. Additionally, in the solution regime, the axial velocity profile displays the crossflow behavior with greater magnetic parameter values. Owing to the enormous advancements in

bioengineering technology, numerous researchers were interested in magnetic fluxes due to their numerous applications. Additionally, by providing a magnetic field, the flow and heat transfer properties are adjusted by the requirements. The concepts of magneto-hydrodynamics, or MHD, are widely used in current biomedicine to treat tiresome disease conditions. These explanations explain why the MHD concept has good practical benefits today. The author [15], conducted a theoretical and experimental examination to examine the impact of magnetic numbers on lubricating flows between two parallel plates. This study [16], used an HPM technique to examine how a magnetic field affected the incompressible two-dimensional Casson fluid flow between two parallel plates. Their analysis demonstrates that the growing magnetic parameter and the decreasing velocity field are related. The influence of the Cattaneo-Christov heat flux model for single- and multi-wall carbon nanotubes on the stagnation point flow of micropolar nanofluid across a stretching surface with slip effects was investigated in [17]. Their study shows that, in the flow zone, the Bejan number is a decreasing function of the Brinkman parameter. The effects of mass flux and Cattaneo-Christov double diffusion heat models on the transient nanofluid flow between two parallel plates with Joule heating and chemical reaction were numerically examined. Their study has noted that the concentration profile is an increasing function of the Brownian motion parameter and a decreasing function of the thermophoresis parameter. In their inquiry showed that the power-law fluid exhibits a dual behavior in the presence of an applied magnetic field, and they also proved the effect of non-uniform heat source on magnetized power-law fluid flow across a stretching sheet with non-Darcian porous medium.

The literature review and the benefits of optimizing flow in multiple scientific and engineering domains, such as biology and biomedicine, served as the authors' driving forces. Because of this, researchers have attempted to examine the behavior of unstable Williamson fluid in terms of flow and heat transfer over a horizontal sensor surface while subjected to external compression and a transverse magnetic field. The current problem is of great interest to engineers, as the literature review has shown.

2 Mathematical Formulations

An investigation is conducted using numerical methods on a two-dimensional mathematical model of magnetized time-dependent, viscous incompressible, electrically conducting Wilson fluid flow around a sensor surface with changing thermal conductivity and external squeezing with viscous dissipation effect. The flow configuration of the current issue (closed compressed channel) is shown in Figure 1 together with all required parameters. Furthermore, let $h(t)$ be the time-dependent height of the closed channel, measured from 0 to h, and be substantially greater than the thickness of the boundary layer. Additionally, the channel encloses the microcantilever sensor of length L, with the lower surface fixed and the upper surface squeezed. It is evident, therefore, that the squeezing action is thought to begin at the tip of the sensor surface and work its way down to the free stream fluid. In addition, the thermodynamic behavior of the current physical situation is addressed with the aid of a well-established rectangular coordinate system in which $x-coordinate$ is taken along axial direction and y-axis is chosen normal to $x-direction$. The fluid flow is driven by the external free stream velocity $U(x,t)$ and the magnetic field of strength Bo is applied normal to the channel.

Equation of continuity:

$$\frac{\partial u}{\partial x}+\frac{\partial v}{\partial y}=0 \tag{1}$$

Momentum equation:

$$\frac{\partial u}{\partial t}+u\frac{\partial u}{\partial x}+v\frac{\partial u}{\partial y} = -\frac{1}{\rho}\frac{\partial P}{\partial x}+\nu\frac{\partial^2 u}{\partial y^2} + 2\nu\Gamma\frac{\partial u}{\partial y}\frac{\partial^2 u}{\partial y^2}-\frac{\sigma {B_0}^2}{\rho}u \tag{2}$$

Free stream equation:

$$\frac{\partial U}{\partial t}+U\frac{\partial U}{\partial x}=-\frac{1}{\rho}\frac{\partial P}{\partial x}-\frac{\sigma {B_0}^2}{\rho}U \tag{3}$$

Energy equation:

$$\left(\frac{\partial T}{\partial t}+u\frac{\partial T}{\partial x}+v\frac{\partial T}{\partial y}\right)=\alpha\ \frac{\partial^2 T}{\partial y^2}+\frac{\mu}{\left(\rho c_p\right)}* \left(1+\Gamma\frac{\partial u}{\partial y}\right)\left(\frac{\partial u}{\partial y}\right)^2 \tag{4}$$

The velocity components along the x and y directions in the Eqs. (1) – (4) are represented by the variables u and v, the free stream velocity

along the axial flow path by U, the fluid temperature by T, the time interval by t, the working fluid density by ρ, the time constant by t, the fixed thermal conductivity by α, the kinematic viscosity of the working liquid by ν, and the magnetic strength by B_0. Eqs. (2) and (4) additionally meet the flow conditions required within the boundary layer region taken into consideration for this investigation. Additionally, the outer free stream flow ($u \to U, v \to 0$), which is presumptively inviscid and uniform about the normal coordinate, is governed by Eq. (3). However, by considering the small sensor length in line with channel height, the mistake in the forecast was eliminated. Lastly, by removing the pressure factor from Eq. (2) and using Eq. (3) as, the necessary flow equation that follows is achieved.

$$\frac{\partial u}{\partial t}u\frac{\partial u}{\partial x}+v\frac{\partial u}{\partial y}=\frac{\partial U}{\partial t}+U\frac{\partial U}{\partial x}+ \nu\frac{\partial^2 u}{\partial y^2}+2v\Gamma\frac{\partial u}{\partial y}\frac{\partial^2 u}{\partial y^2}+\frac{\sigma {B_0}^2}{\rho}(U-u) \quad (5)$$

Therefore, the flow equations (4) and (5) under consideration are simplified about thermal and hydromagnetic circumstances as follows.

$$u|_{y=0}=0,-K\frac{\partial T}{\partial y}\Big|_{y=0}=q(x),v|_{y=0}=V_0, \quad u|_{y=\infty}=U(x,t),T|_{y=\infty}=T_\infty \quad (6)$$

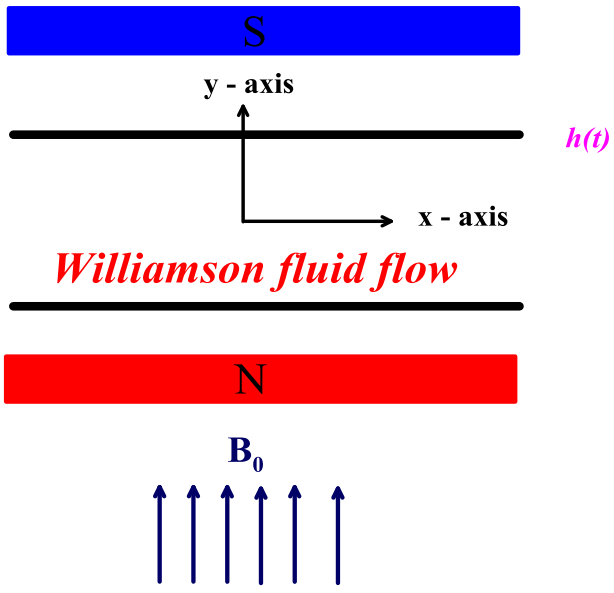

Fig. 1: Physical manifestation of the current issue

The symbols utilized in Eq. (6) are as follows: $q(x)$ represents the surface heat flux, and $U(x,t)$ and T_∞ stands for the ambient fluid velocity and temperature. Furthermore, where is the small quantity in the current situation of the fixed thermal conductivity α Assume that when the wall is thought to be permeable, V_0 describes the reference velocity next to the surface if the sensor surface behaves as a function of the surface heat flow q(x). However, the set of coupled two-dimensional transient Williamson fluid flow Eqs. (4) and (5) with sufficient conditions Eq. (6) are changed into a set of nonlinear ordinary differential equations by applying the proper similarity transformations. Therefore, the following similarity transformations are applied to accomplish this goal.

$$\eta=y\sqrt{\frac{\upsilon_\infty}{a}},u=axf'(\eta),U=ax \quad v=-\sqrt{a\upsilon}\,f(\eta),a=\frac{1}{S+bt} \quad \theta(\eta)=\frac{T-T_\infty}{\left(\frac{q_0 x}{k}\right)\sqrt{\frac{\nu}{\alpha}}},V_0=\frac{v_i}{\sqrt{\nu}} \quad (7)$$

Ultimately, applying Equation (7) to the Eqs. (4) – (6) results in the nondimensional flow system that follows considering η.

$$f'''+\left(\frac{b}{2}\eta+f\right)f''-f'^2+2Wef''f'''+M(1-f')+b(f'-1)+1=0 \quad (8)$$

$$\theta''+Pr\left(\frac{b}{2}\eta+f\right)\theta'-Pr\left(\frac{b}{2}+f'\right)\theta+\Pr Ec\,f''^2+\Pr Ec\,We\;f''^3=0 \quad (9)$$

The modified boundary conditions concerning η are as follows.

$$f(0)=-f_0,f'(0)=0,\theta'(0)=-1 \quad f'(\infty)=1,\theta(\infty)=0 \quad (10)$$

The derivative concerning eta is shown by the superscript "prime" in the Equations (8)– (10). Furthermore, the following definitions apply to the governing physical factors regulating the fluid flow.$M=\frac{\sigma {B_0}^2}{\rho a}$ (Magnetic number), $We=\Gamma U\sqrt{\frac{a}{\nu}}$ (Weissenberg number),b (squeezed flow index), $V_0=\frac{v_i}{\sqrt{\nu}}$ (permeable velocity parameter), $Pr=\frac{\nu}{\alpha}$ (Prandtl number), and $Ec=\frac{U^2}{c_p\left(\frac{q_0 x}{k}\right)\sqrt{\frac{\nu}{\alpha}}}$ (Eckert number).

One dimensionless number that is an inherent characteristic of a fluid is the Prandtl number. Small Prandtl numbers indicate strong thermal conductivity and free flow, making them excellent choices for heat-conducting liquids. Liquid metals

are excellent heat transmission media. It's interesting to note that while common organic solvents are not good heat transfer liquids, air is. The momentum transmission takes precedence over the heat transport as viscosity increases, rendering these liquids unsuitable for heat conduction. For non-Newtonian fluids, the Prandtl number is therefore assumed to be small. The influence of fluid self-heating because of dissipation effects is measured using the Eckert number.

In many technological applications, the engineering numbers of interest, the skin friction coefficient, and heat transfer rate—contribute significantly to the results. As a result, in this work, we have computed computer-generated numerical values for the skin friction coefficient and heat transfer rate, which are reported in Figure 13, Figure14 and Table 1. Nonetheless, the wall shear stress and heat transfer rate are provided below with the aid of defined thermodynamic conditions.

$$Cf = \frac{2\tau_w}{\rho U^2} \tag{11}$$

$$Nux = -\frac{x q_w}{q_0 x \sqrt{\frac{\nu}{a}}} \tag{12}$$

The values of τ_w and q_w in the Eqs. (11) and (12) are determined as follows:

$$\tau_w = \mu_0 \left(\frac{\partial u}{\partial y} + \Gamma \left(\frac{\partial u}{\partial y} \right)^2 \right)_{y=0} \qquad q_w = -k \left(\frac{\partial u}{\partial y} \right)_{y=0} \tag{13}$$

Ultimately, using the similarity variable, the skin-friction coefficient and Nusselt number equations are derived by incorporating Equations (7) and (13) into Equations (11) and (12). This process yields the following results:

$$\frac{1}{2} C_f \sqrt{R_{ex}} = f''(0) + We\left(f''(0)\right)^2 \tag{14}$$

$$Nux(R_{ex})^{-\frac{1}{2}} = -\theta'(0) \tag{15}$$

Therefore, the necessary equations for the skin-friction coefficient and Nusselt number are equations (14) and (15). Additionally, the local Reynolds number is shown by the formulas (14) and (15) above, where $R_{ex} = x\sqrt{\frac{a}{\nu}}$.

3 Analysis of the Results

This section examines how different embedding factors affect the flow of a Williamson fluid over a sensor surface as it is squeezed, considering the Nusselt number, momentum transport coefficient, and temperature and velocity profiles. Additionally, Figure 2, Figure 3, Figure 4, Figure 5, Figure 6, Figure 7, Figure 8, Figure 9, Figure 10, Figure 11 and Figure 12 describe the effects of the Weissenberg number (We), compressed flow index (b), permeability velocity parameter (V_0), magnetic number (M), Eckert number (Ec), and Prandtl number (Pr) on temperature and velocity profiles. Additionally, Table 1, Figure 13, Figure 14 and Figure 15 display the variations in momentum and heat transfer rates observed within the study zone for different values of flow parameters.

Weissenberg number (We)'s effect on $f'(\eta)$ and $\theta(\eta)$:

Figure 2 and Figure 3 show how the Weissenberg number affects the temperature and velocity fields. Figure 2 illustrates how the axial velocity profile decreased as the Weissenberg number increased. The ratio of relaxation time to the process time is known as the physical Weissenberg number. Here, the Weissenberg number magnifying values increase the fluid relaxation time, which strengthens the sensor surface's resistance to the Williamson fluid flow. As a result, this circumstance causes the flow region's resistance to magnify, which lowers velocity as shown in Figure 2. Additionally, Figure 3 shows how the Weissenberg number affects the thermal profile. Figure 3 shows that as the Weissenberg number increases, the temperature field also does, increasing the thickness of the thermal boundary layer in the flow area. As a result, the relationship between temperature and Weissenberg number increases.

Impact of squeezed flow index (b) on $f'(\eta)$ and $\theta(\eta)$:

The effects of b on the temperature field and velocity fields are shown in Figure 4 and Figure 5, respectively. On the other hand, Figure 4 illustrates how the velocity field decreases as the compressed flow index increases. The velocity profile is decreasing because the motion of the Williamson fluid molecules in the flow direction is amplified by an increase in the squeezing process. It is observed that the strength of the squeeze flow and the squeezed flow index have the opposite relationship. As a result, this condition results in a decreased flow velocity increasing b. Additionally, dual velocity behavior is seen in the channel because of the fluctuations at the border. Additionally, Figure 5 shows how b affects the

flow domain's thermal field. It is noteworthy to see that the thermal profile was subdued by the magnification B. Larger b values physically lessen the force that squeezes velocity, which in turn lessens the thermal field. The thickness of the temperature boundary layer decreases as the squeezed flow index increases.

Influence of permeable velocity parameter (V_0) on $f'(\eta)$ and $\theta(\eta)$:

The effect of V_0 on velocity and temperature fields is depicted in Figure 6 and Figure 7, respectively. Figure 6 shows that V_0 increases and decreases the velocity field. This decay in the axial flow field is caused by the fluid being mostly attached to the sensor surface $V_0 > 0$, which is a physical condition that decays the velocity field inside the channel. Additionally, Figure 7 shows that V_0 has an impact on the temperature field. Figure 7 illustrates how the thermal field is enhanced by an increase in the permeability velocity parameter. In this circumstance, the sensor surface's cooling is improved beneath the suction enclosure $V_0 > 0$. In addition, the temperature boundary layer's thickness decreased as the permeability velocity parameter increased.

Effect of Magnetic parameter M on $f'(\eta)$ and $\theta(\eta)$:

The influence of the magnetic parameter on the velocity and heat profiles is shown in Figure 8 and Figure 9, respectively. Figure 8 illustrates how the velocity profile is enhanced by an increase in the magnetic parameter. As a result of the upper plate being squeezed, a rising magnetic parameter physically increases resistance along the axial flow direction. This eliminates the effect of applied magnetic field strength on velocity and increases velocity inside the channel. Additionally, Figure 8 shows that as the magnetic number increases, the velocity boundary layer thickness increases. The impact of magnetic numbers on thermal fields is examined in Figure 9. Figure 9 illustrates how the thermal profile is increased by the increasing Lorentz forces. Furthermore, when the magnetic parameter values increased, so did the thickness of the thermal boundary layer. As a result, the temperature field increases as the magnetic parameter does.

Effect of Prandlt number Pr on $\theta(\eta)$:

Figure 10 show how the Prandtl number (Pr) behaves thermodynamically on a thermal profile. Figure 10 illustrates how Pr affects the thermal field. Figure 10 shows that the thermal profile decays with increasing Pr. The reason for this decline in the thermal profile is because a rise in Pr causes the temperature diffusivity to decrease, which suppresses the thermal field. Additionally, when Pr values increased, the temperature boundary layer's thickness decreased.

Impact of Eckert number Ec on $\theta(\eta)$:

The viscous dissipation effect, which is always positive and indicates a source of heat due to the frictional forces among the fluid particles, is represented by the second term on the right-hand side of Eq. (13). Additionally, the irreversible process known as viscous dissipation converts the work that a fluid performs on nearby fluid layers because of shear forces into heat. In scientific and engineering fields including aerodynamics, injection molding, polymer processing, and others, the viscous dissipation effect has a stronger influence. In real applications, however, boundary layer flows with viscous dissipation effect over sheets/surfaces garner significant attention across a wide range of engineering systems. Figure 11 shows the effect of Eckert number (Ec) on temperature profile. The Eckert number is the primary unit of calculation for heat dissipation in the specified physical system. When the Eckert number is higher than the enthalpy changes in each physical system or medium, it indicates the advective transport mechanism, which has a significant impact on heat transfer phenomena. Nevertheless, Figure 11 shows that the thermal profile increases when the Eckert number increases. Ec directly affects the mechanism of heat dissipation, which strengthens the thermal field, making the increase in temperature evident. Additionally, as the Eckert number increases, the thickness of the thermal boundary layer decreases.

Skin-friction coefficient and Nusselt number behavior

Table 1, Figure 12 and Figure 13 show how different control settings affect the skin friction coefficient and Nusselt number. The skin-friction coefficient numerical values produced by the computer for a range of flow parameter values are tabulated in Table 1. On the other hand, Table 1 makes it evident that while improving b reduces the skin friction coefficient, raising We and M values increases it. Additionally, the skin-friction coefficient increases for $V_0 < 0$and decreases for $V_0 > 0$. Furthermore, because Pr and Ec are not explicitly included in the momentum equation, they

have no discernible impact on the skin friction coefficient.

In a similar vein, Figure 12 and Figure 13 show how b, V_0 affect the profile of heat transfer rate. Because both the temperature boundary condition (see Eq. (10)) and the heat transfer rate formula (see Eq. (15) start with a negative sign, Figure 12 and Figure 13 also start with negative values. Figure 12 clearly shows that as values of b grow, the thermal barrier layer thickness reduces while the increased squeezed flow index increases the rate of heat transmission. Physically, by creating high heat molecular forces and high pressure on the fluid flow, increasing the squeezed flow index enhances the rate of heat transmission. Furthermore, Figure 13 shows that the permeability velocity parameter decreases as the heat transfer rate profile increases. Additionally, when the values of V_0 grow, so does the thickness of the thermal boundary layer.

4 Conclusion

A numerical study is conducted on a two-dimensional magnetized Williamson fluid flow surrounding a sensor surface that has variable thermal conductivity and external squeezing with a viscous dissipation effect. The time-dependent coupled nonlinear partial differential equations resulting from the examined physical problem are reduced to ordinary differential equations by the incorporation of appropriate similarity transformations. Using the shot technique and the Runge-Kutta fourth-order integration scheme, the resulting nonlinear flow system is solved. By performing the parametric analysis relating to the numerous physical parameters, the physics underlying the current situation is unearthed. The temperature behavior and flow sensitivity of the Williamson fluid around a sensor surface are depicted in the tables and graphs. The following is a limited list of the key findings related to the current numerical study:

- ✓ As the Weissenberg number increases, the thickness of the momentum boundary layer is observed to decrease.
- ✓ As the Weissenberg number increases, so does the temperature profile.
- ✓ Temperature and velocity fields were suppressed as the compressed flow index increased.
- ✓ The velocity profile became less as the permeability velocity parameter increased. On the temperature profile, however, the opposite tendency is seen.
- ✓ As the Eckert number climbed, so did the thermal profile.
- ✓ The momentum transmission coefficient increased as the magnetic parameter and Weissenberg number increased. However, the increasing compressed flow indicator shows the opposite trend.
- ✓ Science and engineering-related flow issues can be effectively resolved by using the Runge-Kutta scheme and firing approach.
- ✓ The Nusselt number's magnitude rises as V_0 values rise.

Furthermore, a wide range of commercial applications, including solar collectors, fluidic cells for thermal flow, oil recovery, and so on, are predicted to benefit from the current numerical analysis.

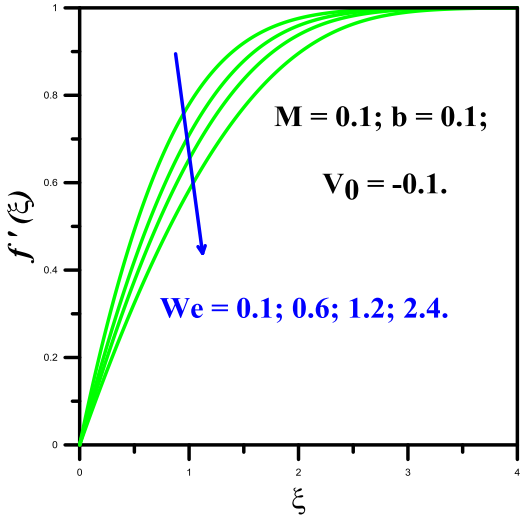

Fig. 2: Effect of We on $f'(\xi)$

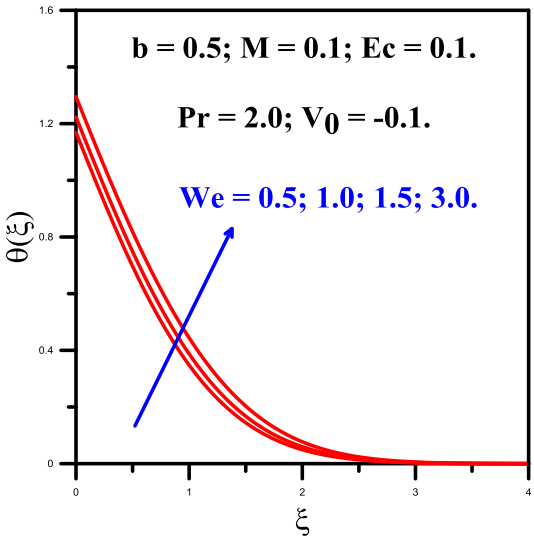

Fig. 3: Effect of We on θ(ξ)

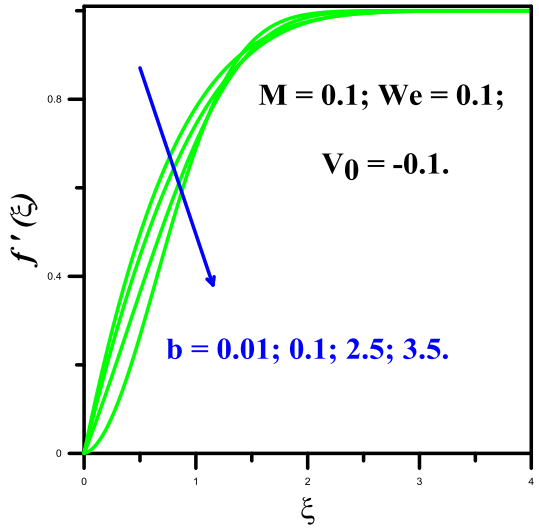

Fig. 4: Effect of b on $f'(\xi)$

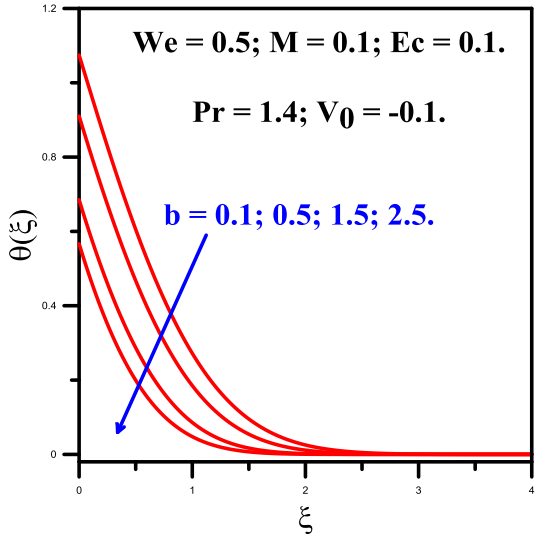

Fig. 5: Effect of b on $\theta(\xi)$

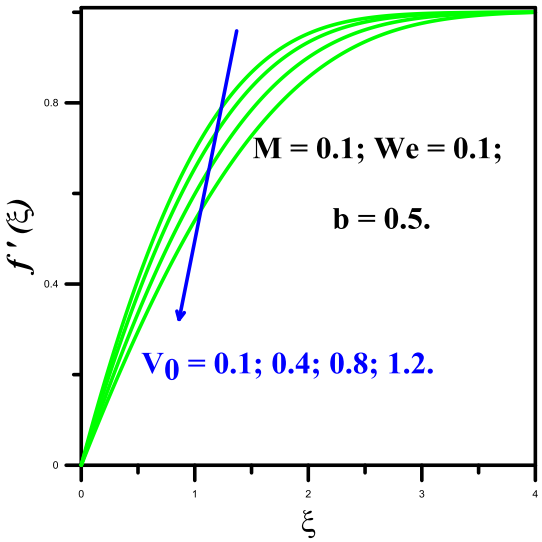

Fig. 6: Effect of V_0 on $f'(\xi)$

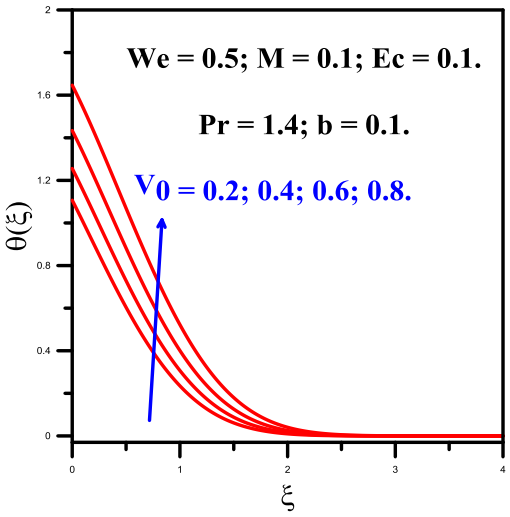

Fig. 7: Effect of V_0 on $\theta(\xi)$

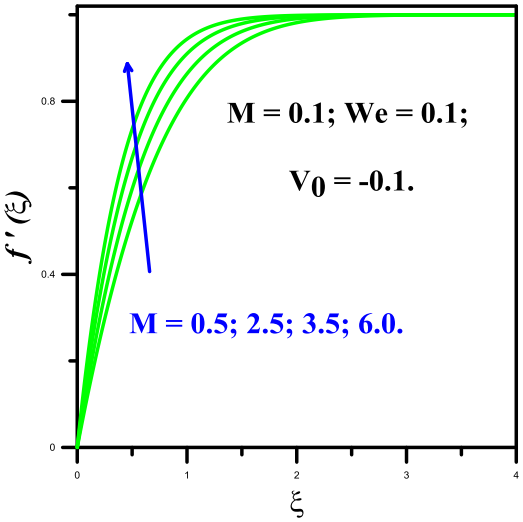

Fig. 8: Effect of M on $f'(\xi)$

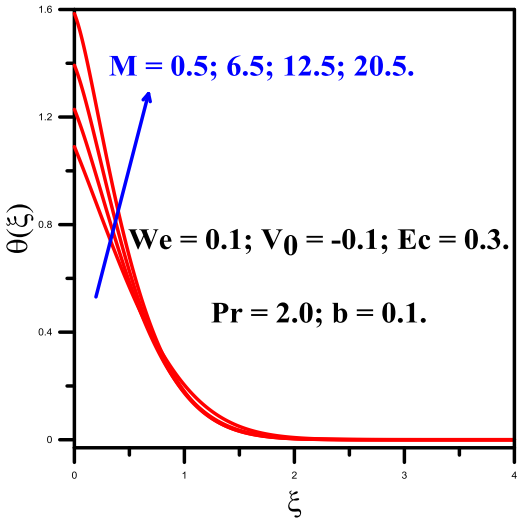

Fig. 9: Effect of M on $\theta(\xi)$

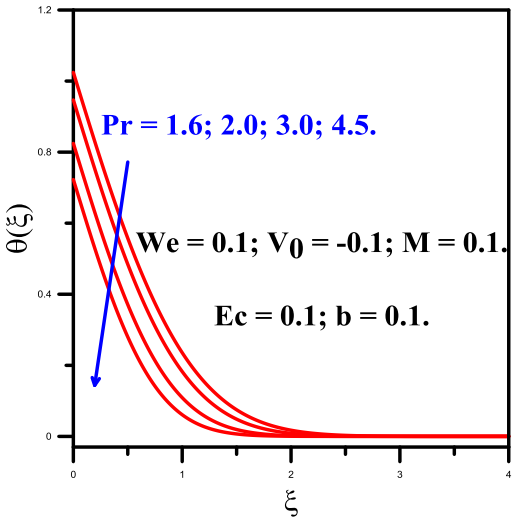

Fig. 10: Effect of Pr on $\theta(\xi)$

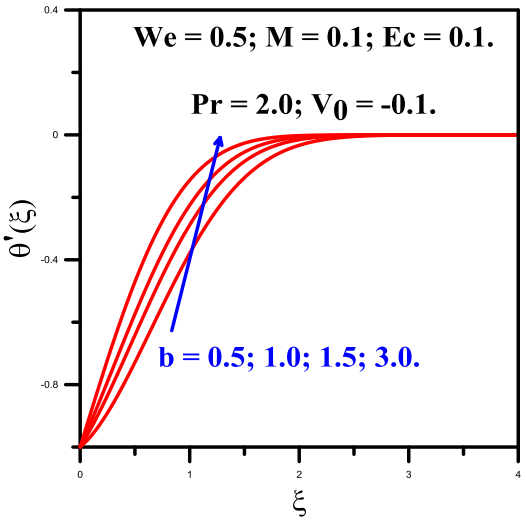

Fig. 12: Effect of b on $\theta'(\xi)$

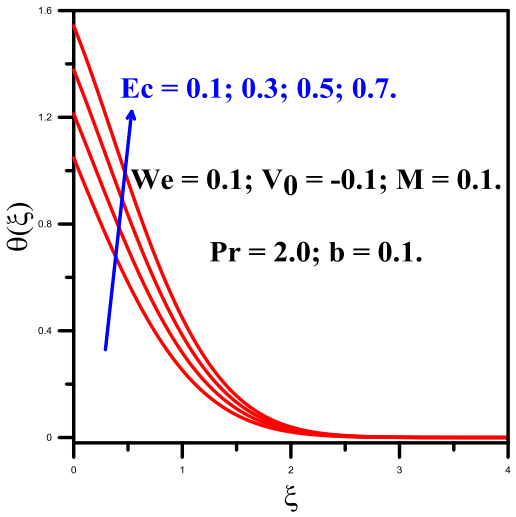

Fig. 11: Effect of Ec on $\theta(\xi)$

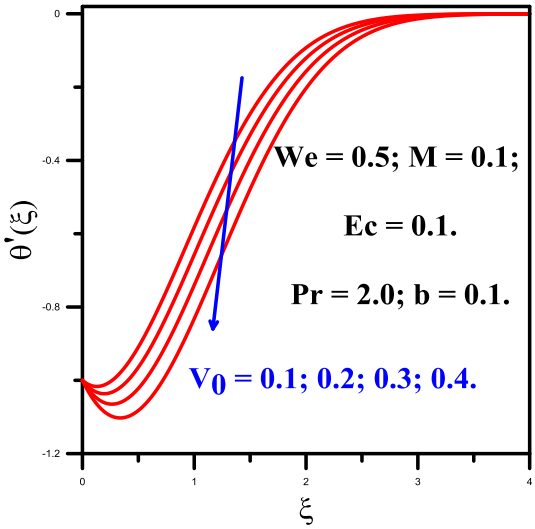

Fig. 13: Effect of V_0 on $\theta'(\xi)$

Table 1. Numerical values of the momentum transmission coefficient produced by a computer for various flow parameter values

We	b	M	V_0	$f''(0)+We(f''(0))^2$
0.1	0.3	0.3	−0.3	1.50414380620
0.3				1.59435084092
0.5				1.66892373828
0.7				1.73365261481
0.7	0.0			1.83582405994
	0.1			1.80199869624
	0.2			1.76794227685
	0.3			1.73365261481
0.9		0.1	0.9	1.90547277814
		0.3		2.01666361026
		0.5		2.12350414387
		0.7		2.22652118285
0.8			−0.7	2.10274588281
			−0.6	2.05949892350
			−0.5	1.98918344121
			0.0	1.65452384436
			+0.5	1.35196071986
			+0.6	1.29576833263
			+0.7	1.24111065073

References:

[1] Lawal A, Kalyon DM. Squeezing flow of viscoplastic fluids subject to wall slip. *Polym Eng Sci.*, 1998;38(11):1793–804.

[2] Xu C, Yuan L, Xu Y, Hang W. Squeeze flow of interstitial Herschel-Bulkley fluid between two rigid spheres. *Particuology*. 2010;8 (4):360–4.

[3] Engmann J, Servais C, Burbidge AS. Squeeze flow theory and applications to rheometry: A review. *J Non-Newt Fluid Mech*., 2005;132(1-3):1–27.

[4] Zhang X, Ju H, Wang J. *Electrochemical sensors, biosensors, and their biomedical applications*. USA: Academic Press; 2008.

[5] Lavrik NV, Tipple CA, Sepaniak MJ, Datskos D. Gold-nano structures for transduction of Biomolecular interactions into scale micrometer-scale movements. *Biomed Microdevices*. 2001;3(1):35–44.

[6] Stefan M. J., Experiment on apparent adhesion, session report-SächsAkadWissWein, Math-Nat. Know. Kl. 1874; 69: 713–21. (Stefan MJ. Versuchüber die scheinbare adhesion, Sitzungsber-SächsAkadWissWein), Math-Nat. Wiss.

[7] Wang CY, Watson LT. Squeezing of a viscous fluid between elliptic plates. *Appl Sci Res.*, 1979;35(2-3):195–207.

[8] Bhattacharyya S, Pal A. Unsteady MHD squeezing flow between two parallel rotating Discs. *Mech Res Commun.*, 1997;24(6):615–23.

[9] Siddiqui AM, Irum S, Ansari AR. Unsteady squeezing flow of a viscous MHD fluid between parallel plates, a solution using the homotopy perturbation method. *Math Model Anal.*, 2008; 13(4):565–76.

[10] Rashidi MM, Siddiqui AM, Rastegari MT. Analytical solution of squeezing flow between two circular plates. *Int J Comput Methods Eng Sci Mech.*, 2012;13(5):342–9.

[11] Mustafa M, Hayat T, Obaidat S. On heat and mass transfer in the unsteady squeezing flow between parallel plates. *Meccanica*. 2012; 47(7):1581–9.

[12] Hayat T, Sajjad R, Alsaedi A, Muhammad T, Ellahi R. On the squeezed flow of couple stress nanofluid between two parallel plates. *Results Phys.*, 2017; 7:553–61.

[13] Maki ER, Kuzma DC, Donnelly RJ. Magneto-hydrodynamic lubrication flow between parallel plates. *J Fluid Mech.*, 1966; 26(3):537–43.

[14] Khan M, Qayyum M, Khan O, Ali M. Unsteady squeezing flow of Casson fluid with magneto-hydrodynamic effect and passing through a porous medium. *Math Probl Eng.*, 2016; 2016:1–14.

[15] Ahmad S., Nadeem S., Muhammad N., Khan M.N., Cattaneo– Christov heat flux model for stagnation point flow of micropolar nanofluid toward a nonlinear stretching surface with slip e_ects, *J. Therm. An. Calorim.*, 2020, https://doi.org/10.1007/s10973-020-09504-2.

[16] Shankar U, Naduvinamani NB, Basha H. A generalized perspective of Fourier and Fick's laws: magnetized effects of Cattaneo-Christov models on the transient nanofluid flow between two parallel plates with Brownian motion and thermophoresis. *Nonlinear Eng.*, 2020;9(1):201–22.

[17] Mishra SR, Baag S, Dash GC, Acharya MR. Numerical approach to MHD flow of power-law fluid on a stretching sheet with nonuniform heat source. *Nonlinear Eng.*, 2019; 9(1):81–93.

Contribution of Individual Authors to the Creation of a Scientific Article (Ghostwriting Policy)

A. EL Harfouf: Conceptualization, Formal analysis, Investigation, Methodology, Project administration, Resources, Validation, Writing – original draft, Data curation, Software, Visualization. **R. Herbazi:** Conceptualization, Formal analysis, Investigation, Methodology, Project administration, Resources, Validation, Writing – review & editing. **S. Hayani Mounir:** Conceptualization, Investigation, Project administration, Writing – review & editing. **H. Mes-adi:** Conceptualization, Formal analysis, Investigation, Methodology, Project administration, Resources, Validation, Writing – review & editing. **A. Wakif:** Conceptualization, Investigation, Project administration, Supervision, Writing – review & editing.

Sources of Funding for Research Presented in a Scientific Article or Scientific Article Itself

No funding was received for conducting this study.

Conflict of Interest

The authors have no conflicts of interest to declare.